

## Article

# Low-Temperature Gas Cooling Correction Trajectory Offset Technology of Laser-Induced Thermal Crack Propagation for Asymmetric Linear Cutting Glass

Chunyang Zhao <sup>1</sup>, Zhihui Yang <sup>1</sup>, Xiuhong Qiu <sup>1</sup>, Jiayan Sun <sup>1</sup>  and Zejia Zhao <sup>1,2,\*</sup>

<sup>1</sup> Guangdong Provincial Key Laboratory of Micro/Nano Optomechatronics Engineering, College of Mechatronics and Control Engineering, Shenzhen University, Shenzhen 518060, China; zcy724317@163.com (C.Z.); 15007960781@163.com (Z.Y.); 18916536921@163.com (X.Q.); sunjiayan730@163.com (J.S.)

<sup>2</sup> Institute of Semiconductor Manufacturing Research, College of Mechatronics and Control Engineering, Shenzhen University, Shenzhen 518060, China

\* Correspondence: zhaozejia@szu.edu.cn

**Abstract:** Laser-induced thermal crack propagation (LITP) is a high-quality and efficient processing method that has been widely used in fields such as glass cutting. However, the problem of trajectory deviation often arises in actual cutting operations, especially in asymmetric cutting. To address this issue, a low-temperature gas cooling trajectory deviation correction technique was proposed in this study. This technique modifies the temperature and stress distribution by spraying low-temperature gas onto the processing surface and maintaining a relative position with the laser, thereby correcting the trajectory deviation. The finite element simulation software ABAQUS was employed to numerically simulate the dynamic propagation of temperature fields, thermal stress, and cracks in the asymmetric linear cutting and circular cutting of soda-lime glass with the proposed low-temperature gas cooling trajectory deviation correction technique, and the correction mechanism was elucidated. In the simulation results, the optimal relative distance ( $\Delta X$ ) between the low-temperature gas and scanning laser was obtained by analyzing the transverse tensile stress. Based on the analysis of the experimental and numerical simulation results, it is concluded that the cryogenic gas cooling technique can effectively correct the trajectory deviation phenomenon of asymmetric linear cutting of soda lime glass by LITP.

**Keywords:** low-temperature gas cooling technology; laser-induced thermal crack propagation (LITP); soda-lime glass; track correction



**Citation:** Zhao, C.; Yang, Z.; Qiu, X.; Sun, J.; Zhao, Z. Low-Temperature Gas Cooling Correction Trajectory Offset Technology of Laser-Induced Thermal Crack Propagation for Asymmetric Linear Cutting Glass. *Processes* **2023**, *11*, 1493. <https://doi.org/10.3390/pr11051493>

Academic Editor: Hideki KITA

Received: 17 April 2023

Revised: 3 May 2023

Accepted: 10 May 2023

Published: 15 May 2023



**Copyright:** © 2023 by the authors. Licensee MDPI, Basel, Switzerland. This article is an open access article distributed under the terms and conditions of the Creative Commons Attribution (CC BY) license (<https://creativecommons.org/licenses/by/4.0/>).

## 1. Introduction

As a brittle material, glass has been widely utilized in various electronic device screens due to its high transparency, high mechanical strength, uniform texture, smooth surface, and corrosion resistance. With the popularity of smartphones, handheld devices, and tablet computers, the demand for high-quality, high-efficiency, and high-strength glass cutting has been increasing, which has become an important technological challenge in the glass manufacturing industry [1–4].

At present, the conventional mechanical cutting method is widely employed to cut glass, which involves the use of hard metal tools and physical contact force between them and the glass [5]. C.T. Pan et al. [6] proposed that the size of the median crack increases with the increase of cutting depth and cutting pressure, but an appropriate size of the median crack can eliminate edge chipping and obtain a smooth separation surface. M. Zhou et al. [7] demonstrated that adding ultrasonic vibration to diamond cutting during glass cutting can effectively reduce tool wear and improve the surface finish, which has been verified by experiments. Although this contact scratching method often generates many

microcracks and small chippings on the cutting edge, these microcracks may propagate under continuous forces in the subsequent processing, leading to a rapid decrease in the number of products.

Therefore, traditional mechanical cutting methods are gradually being replaced by non-traditional cutting methods [8–10]. Finding a suitable cutting technology with high quality and efficiency has become an urgent issue [11,12]. Laser-induced thermal crack propagation (LITP) is a non-traditional and competitive glass processing method with features of non-contact, high-quality, high-efficiency, and high-strength processing [13]. Lumley [14] proposed LITP for cutting brittle materials. Laser-induced thermal crack propagation involves a laser instead of a tool in a non-contact form. The cut section is smooth, clean, and straight, free of contamination and defects, and extremely strong. The material only undergoes separation but is not removed during the crack propagation process, which not only avoids material damage but also greatly improves the material utilization efficiency. Therefore, laser-induced thermal crack propagation is widely recognized as the method with the highest cross-section quality for glass cutting [15,16].

H.S. Kang et al. conducted a study on laser-induced thermal crack propagation for liquid crystal displays (LCDs), plasma displays (PDPs), and flat panel displays (FPDs). The results showed that the uneven distribution of the liquid after being sprayed onto the glass surface resulted in poorer edge quality when using liquid cooling for glass cutting compared to gas cooling [17]. C.H. Tsai et al. [18] used a diamond tool to scribe and scanned along the scribe with a continuous CO<sub>2</sub> laser. They found that the uncertainty of the size and direction of cracks at the bottom of the scribe resulted in the separated surface after processing not being perpendicular to the surface of the flat glass. Salman Nisar et al. [19] conducted a study on symmetrically cutting glass using diode laser-induced thermal crack propagation. The results showed that there was a serious trajectory deviation phenomenon at the entry and exit points of the material. During the stable cutting stage, the crack could extend along the trajectory of the laser movement.

However, asymmetric linear cutting (where the cut line does not coincide with the material centerline, including asymmetric straight lines and circular curves) is more common in practical processing. The asymmetry of the material on both sides of the scan line causes the stress distribution asymmetry and the location of the shear minimum does not appear on the scan line, causing the crack trajectory to be shifted; while the trajectory shifting mechanism of circular curve cutting also includes the effect of the asymmetry of the temperature field distribution and the hysteresis of crack expansion, causing the crack trajectory to be shifted. C.Y. Zhao et al. [20] proposed a dual-beam laser trajectory offset correction technique that can effectively correct the trajectory offset phenomenon that occurs when cutting asymmetric glass by laser-induced thermal crack propagation. However, this technique increases the complexity and cost of the equipment and raises the maximum temperature of the material during the cutting process, which may lead to defects in the material separation surface. In addition, the technique is better for the correction of asymmetric straight lines but is less effective for the correction of trajectory offsets with small cutting arc radii.

In this study, a cryogenic gas cooling trajectory deviation correction technique is proposed to solve the trajectory deviation problem in asymmetric cutting. The technique involves directing the cryogenic gas to the side where the temperature gradient needs to be increased in order to change the temperature and stress distribution. Numerical simulations were performed to investigate the temperature field, thermal stresses, and dynamic crack expansion during the correction of a cryogenic gas cooling trajectory deviation for the asymmetric linear cutting of glass. The optimal relative distance ( $\Delta X$ ) between the cryogenic gas and the scanning laser was obtained by combining the experimental results and simulation data. The correction mechanism of the cryogenic gas cooling trajectory deviation correction technique is further explained.

## 2. Theoretical and Simulation Models

The principle of the low-temperature gas cooling trajectory deviation correction technique is to direct low-temperature gas towards the side that requires an increase in the temperature gradient to form a larger temperature gradient and reduce asymmetric stress, thereby reducing the trajectory deviation. As the gas jet generates a significant amount of pressure, the same arrangement strategy is employed to symmetrically place the nozzle on the upper and lower sides of the specimen to shield the effect of the jet pressure on processing, ensuring that the pressure on both sides of the material is consistent during jetting (as shown in Figure 1).

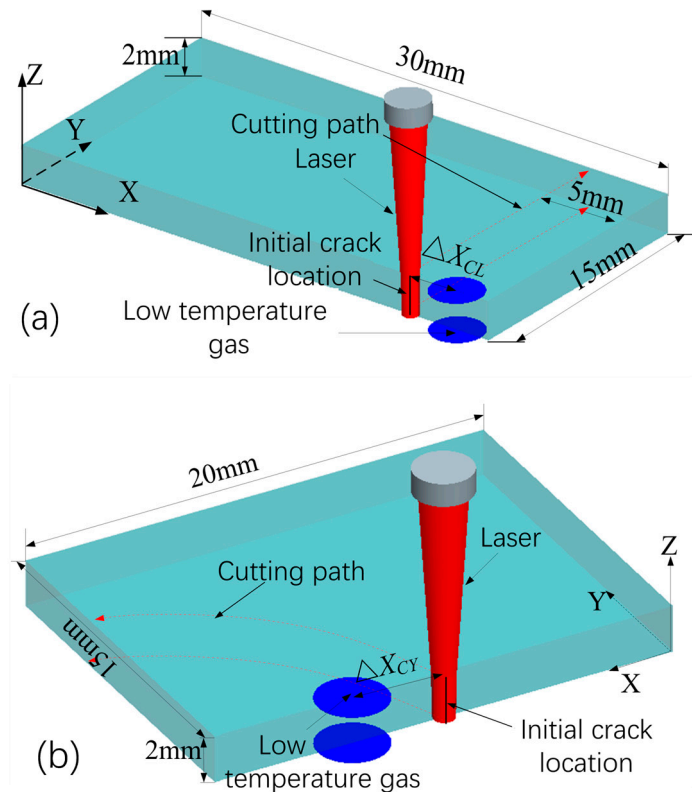


**Figure 1.** Low-temperature gas cooled revising the trajectory deviation technology. (a) Asymmetric line. (b) Circular arc curve.

Upon the laser entering the scanning area, the material temperature rapidly drops, leading to material shrinkage and tensile stress. In the case of laser scanning on asymmetric glass, the asymmetric thermal stress can cause a trajectory deviation. Therefore, low-temperature gas jetting to the side that requires an increased temperature gradient can improve the symmetry of the cutting process and reduce the trajectory deviation. For asymmetric linear cutting, low-temperature gas jetting should be applied to the side with less material to correct the trajectory. For circular arc cutting, low-temperature gas jetting should be applied to the side that requires an increased temperature gradient on the inner side of the arc to correct the trajectory.

The absorption mode of sodium–calcium flat glass for a continuous semiconductor laser with a wavelength of 1064 nm is in the bulk absorption mode, as shown in Figure 2. The expression for the planar Gaussian distribution cone divergent bulk absorption heat source with uniform linear motion can be represented by Equation (1) [21,22].

$$q_G(x, y, z) = \frac{2(1 - R_G) \cdot \alpha \cdot P_0}{\pi[r_G + (H_G - z)\tan\theta/2]^2} \cdot e^{-\alpha \cdot (H_G - z)} \cdot e^{-\frac{(x-x_0-vt)^2 - (y-y_0)^2}{[r_G + (H_G - z)\tan\theta/2]^2}} \quad (1)$$

where  $x_0, y_0$  are the position coordinates of the scanning start beam center;  $q_G$  is the heat flux function of the heat source in the glass;  $R_G$  is the reflectance of the 1064 nm laser incident on the air–glass interface;  $P_0$  is the laser power;  $H_G$  is the thickness of the glass layer;  $r_G$  is the spot radius of the laser beam at the outer surface of the glass layer;  $\theta$  is the divergence angle of the laser beam; and  $v$  is the scanning speed.

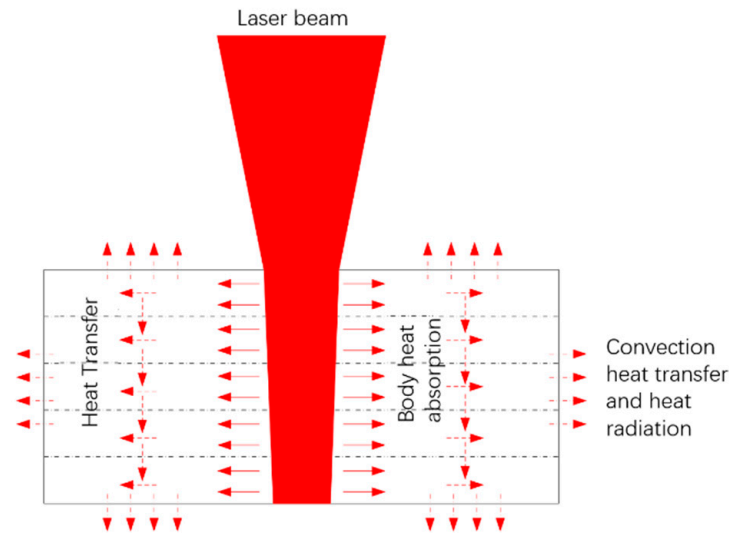


**Figure 2.** The schematic of the laser irradiates the glass–silicon double layer wafer.

For isotropic and homogeneous materials, the temperature field  $T(x, y, z, T)$  is obtained using a transient solver program controlled by the heat diffusion in Equations (2)–(4) based on the conservation of energy and Fourier’s law in the Cartesian coordinate system.

$$k \left( \frac{\partial^2 T}{\partial^2 x} + \frac{\partial^2 T}{\partial^2 y} + \frac{\partial^2 T}{\partial^2 z} \right) + Q = \rho C \cdot \frac{\partial T}{\partial t} \quad (2)$$

$$T(x, y, z, 0) = 20 \text{ } ^\circ\text{C} \quad (3)$$

$$-k \left( \frac{\partial T}{\partial n} \right)_W = h(t_W - t_f) \quad (4)$$

where  $k, Q, \rho$  are the thermal conductivity, heat generated per unit volume of laser irradiation and the specific heat. It is assumed that the initial temperature of the glass is at room temperature of 20 °C,  $W$  is the thermal convection surface between the outside air and the glass, and  $h$  is the glass, the convection coefficient between the outside air and the glass.

To investigate the effect of low-temperature gas cooling on trajectory correction, the flow field distribution of the gas jet injected onto a flat plate was simulated using the FLUENT simulation software. The numerical solution of the heat transfer coefficient distribution on the flat plate was obtained through the simulation, and an approximate analytical solution for the heat transfer coefficient distribution was obtained by fitting the numerical solution using MATLAB.

During the FLUENT simulation process, the RNG  $k$ - $\epsilon$  model was used to investigate the impinging flow of a single circular jet [23–25]. The nozzle was perpendicular to the material surface, and the model and mesh division is shown in Figure 3, where  $H/D = 10$ . The boundary condition was  $Re = 14,000$ , the indoor temperature was  $T = 300$  K, the solid wall was a non-slip boundary, and the injection method was a fixed-point injection. The heat transfer coefficient distribution cloud map on the solid wall was extracted (as shown in Figure 4), and the heat transfer coefficient on the centerline was obtained and curve-fitted using MATLAB (as shown in Figure 5). The R-square value after fitting was 0.951,

indicating that a good fitting curve can be obtained through Gaussian fitting. The final analytical solution for the fitted curve is Equation (5).

$$H = 443.4 \exp\left(-\frac{x^2}{0.00145^2}\right) \quad (5)$$

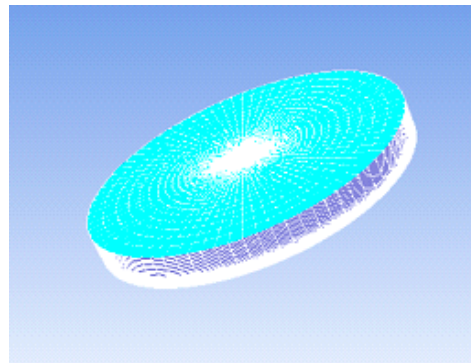


Figure 3. Model and mesh generation.

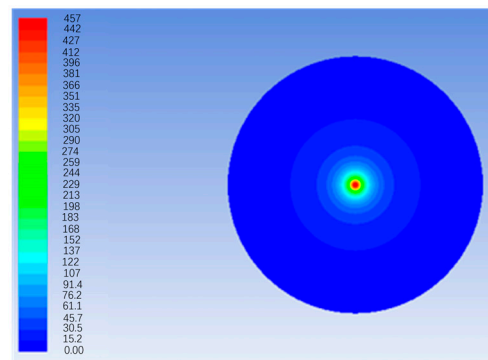


Figure 4. Heat transfer coefficient distribution.

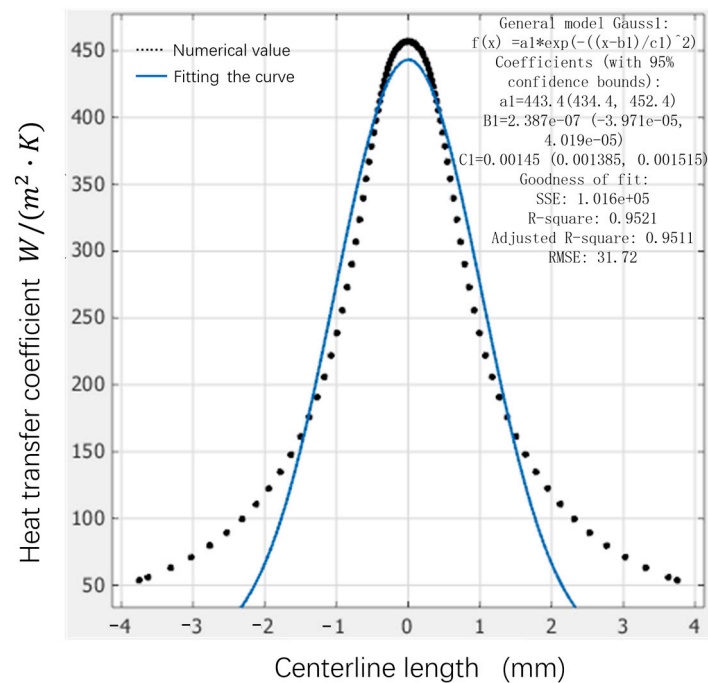
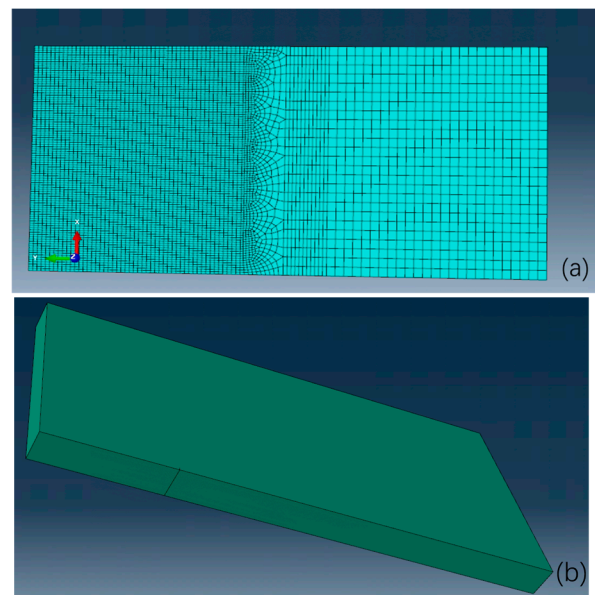


Figure 5. The fitted curve of heat transfer coefficient.

By injecting cryogenic gas, the local convective heat transfer coefficient can be increased and the local temperature of the material can be reduced, thus changing the distribution of the temperature field. Using the approximate analytical solution of the heat transfer coefficient distribution obtained above, it is introduced into the ABAQUS user subroutine for solving the analytical model of the temperature field and studying the effect of the relative position between the center position of the jet and the center position of the laser spot on the temperature field distribution.

The sequential coupled thermoelastic and extended finite element method (XFEM) analysis was conducted using the ABAQUS software, with a modeled size of 30 mm × 15 mm × 2 mm. The mesh and initial crack state (200 μm) of the specimen are illustrated in Figure 6. The total number of elements used was 63,720.



**Figure 6.** Mesh of the specimen and the initial crack state. (a) Mesh of the specimen; (b) initial crack state.

In asymmetric cutting, both the crack extension direction and the crack plane may be deflected, and these two types of deflection (as shown in Figure 7) are tilt type and twist type, respectively. The tilt type means that the crack plane is rotated around the  $O_z$  axis by  $\theta$  (tilt angle), and the rotation of the crack face in the  $\theta$  direction is achieved by continuous adjustment of the crack leading edge; the twist type means that the crack plane is rotated around the  $O_x$  axis by  $\phi$  (twist angle), and the rotation of the crack face in the  $\phi$  direction is achieved by “step” splitting of the crack leading edge. The main type of deflection is tilted, and it is the transverse shear stress that affects the direction of crack expansion in asymmetric cuts.

$$\left. \begin{aligned} \sigma_{y'y'} &= \sigma_{\theta\theta}^I + \sigma_{\theta\theta}^{II} = [K_I / (2\pi r)^{1/2}] f_{\theta\theta}^I + [K_{II} / (2\pi r)^{1/2}] f_{\theta\theta}^{II} = K_I'(\theta) / (2\pi r)^{1/2} \\ \tau_{x'y'} &= \sigma_{r\theta}^I + \sigma_{r\theta}^{II} = [K_I / (2\pi r)^{1/2}] f_{r\theta}^I + [K_{II} / (2\pi r)^{1/2}] f_{r\theta}^{II} = K_{II}'(\theta) / (2\pi r)^{1/2} \\ \tau_{x'z'} &= 0 \end{aligned} \right\} \quad (6)$$

$$\left. \begin{aligned} \sigma_{y'y'} &= \sigma_{\phi\phi}^I + \sigma_{\phi\phi}^{III} = [K_I / (2\pi r)^{1/2}] g_{\phi\phi}^I = K_I'(\phi) / (2\pi r)^{1/2} \\ \tau_{x'y'} &= 0 \\ \tau_{x'z'} &= \tau_{z'\phi}^I + \tau_{z'\phi}^{III} = [K_{III} / (2\pi r)^{1/2}] g_{z'\phi}^{III} = K_{III}'(\phi) / (2\pi r)^{1/2} \end{aligned} \right\} \quad (7)$$

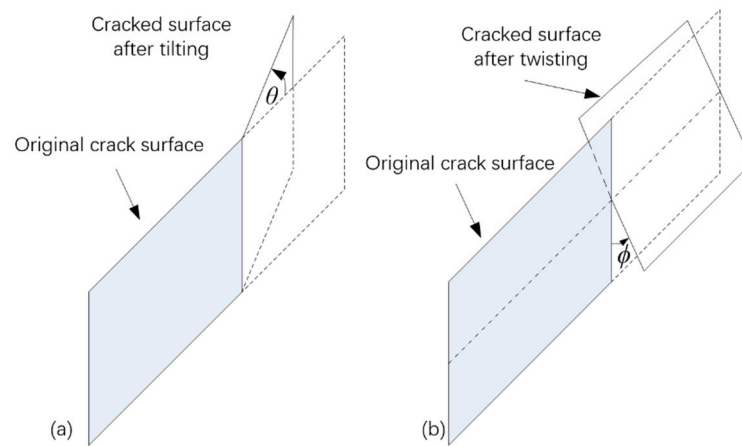


**Figure 7.** Model of crack nonplanar extension (a) sloping type; (b) distortion type.

### 3. Experimental Steps

In the trajectory offset correction technique with cryogenic gas cooling, the schematic diagram of the trajectory correction system is shown in Figure 8. The equipment used in this study is a fiber-coupled 300 W continuous-wave, diode-pumped, solid-state laser with a wavelength of 1064 nm, and the specifications of the main lasers used in the experiment are shown in Table 1. The gas pump (The gas flow rate is 5 L/min) is placed in a space with an ambient temperature of  $-20\text{ }^{\circ}\text{C}$ . The gas was fed through a tee and a gas guide tube, which was fixed to the machine through a snakeskin tube, and the relative positions of the laser and the jet were adjusted by an XY trimmer table. To ensure that the two lasers irradiate vertically onto the material surface, the two lasers are arranged on either side of the material. The material is placed above the focal point and the distance to the focusing lens is varied to obtain the desired laser beam size on the material surface.

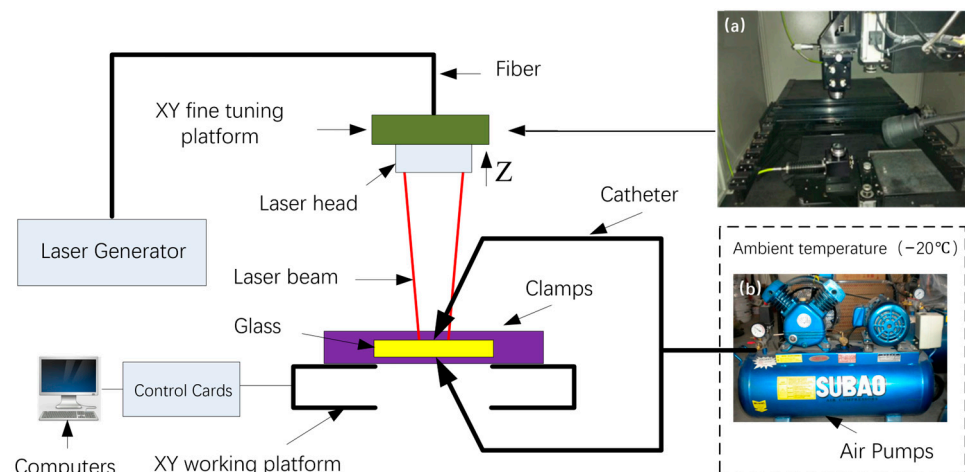


**Figure 8.** Experimental setup for cryogenic gas cooling trajectory correction technology during asymmetric cutting with LITP technology. (a) Diagram of laser and experimental setup equipment, (b) diagram of air pump equipment.

**Table 1.** The main parameters of the laser used in the experiment.

Laser beam wavelength	(nm)	1064
Range of output power	(W)	0–300
Launch angle	(mrad)	$\leq 10$
Beam mode		$TEM_{00}$
Output mode		Continuous
Output power stability	(RMS)	$\leq 2\%$

The specimens used were soda-lime flat glass with a sample size of  $30 \times 15 \times 2 \text{ mm}^3$ . The physical properties are shown in Table 2. An initial crack of more than  $200 \text{ }\mu\text{m}$  was prefabricated on the edge of the glass sample with a diamond wire saw. The best cutting quality was achieved at this time when the laser scanning trajectory was at a distance  $\Delta L = 5 \text{ mm}$  from the nearest edge of the specimen, and the processing parameters were laser power  $P = 30 \text{ W}$ , scanning speed  $V = 4 \text{ mm/s}$ , and spot diameter  $D = 2 \text{ mm}$ , while in the circular curve cutting process, the specimen size was  $20 \times 15 \times 2 \text{ mm}^3$  and the cutting arc radius  $R = 10 \text{ mm}$ , and the processing parameters were laser power  $P = 30 \text{ W}$ , scanning speed  $V = 3 \text{ mm/s}$ , and spot diameter  $D = 3 \text{ mm}$ .

**Table 2.** Physical properties of soda-lime glass.

Density	$D \text{ (kg/m}^3\text{)}$	2480
Thermal Conductivity	$\lambda \text{ (W/m}\cdot\text{°C)}$	0.8
Specific Heat	$C \text{ (J/kg}\cdot\text{°C)}$	836
Poisson's Ratio	$\xi$	0.23
Young's Modulus	$\text{(GPa)}$	74
Expansion coefficient	$\alpha \text{ (10}^{-6}\text{/°C)}$	9.1
Fracture toughness	$\text{(MPa m}^{1/2}\text{)}$	30

#### 4. Results

Figure 9 shows the temperature field distribution during asymmetric cutting. When the relative distance between the laser spot and the jet center is  $\Delta X_{CL} = \Delta X_{CY} = 0.7 \text{ mm}$ , the temperature distribution of the low-temperature gas-cooling trajectory correction technique is shown in Figure 10. It can be observed that introducing low-temperature gas on the right side of the scanning line during the trajectory correction process of the asymmetric straight cutting path using low-temperature gas cooling reduces the temperature in that area, and the highest temperature of the specimen is lower than that without correction. The same effect is achieved when introducing low-temperature gas on the inner side of the scanning line for trajectory correction during circular arc cutting with low-temperature gas cooling.

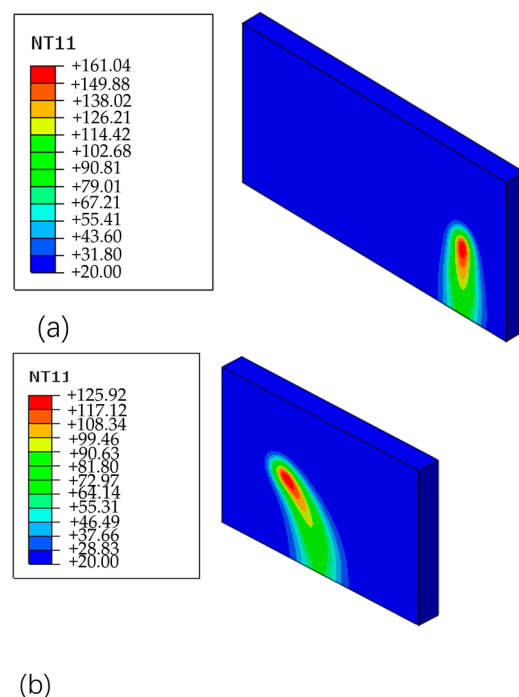


**Figure 9.** Temperature field distribution of asymmetric cutting. (a) Asymmetric line; (b) circular arc curve.

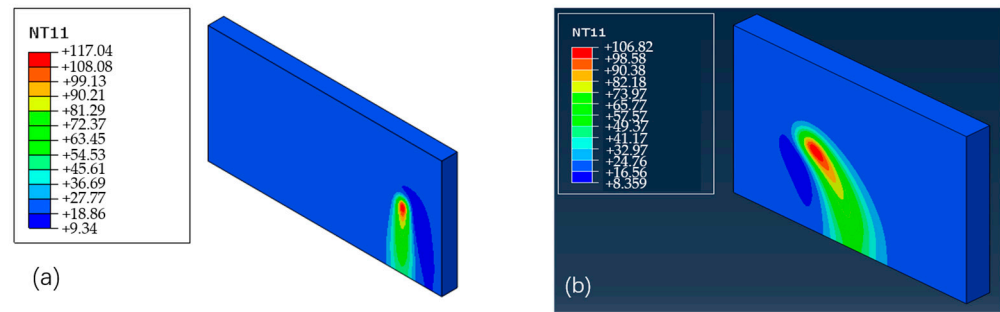


**Figure 10.** Temperature field distributions of low-temperature gas cooled revising the trajectory deviation. (a) Asymmetric line; (b) circular arc curve.

Figure 11a shows the influence of the relative distance  $\Delta X_{CL}$  between the laser spot center and the jet center on the temperature distribution perpendicular to the scanning direction at the crack front during the process of correcting the asymmetric straight cutting path using low-temperature gas cooling when the laser is scanned to 10 mm. It can be observed that the highest material temperature always appears on the laser scanning line, and as  $\Delta X_{CL}$  increases, the highest temperature gradually increases, and the temperature gradient on the left side of the scanning line changes less than that on the right side. However, when  $\Delta X_{CL}$  further increases to 1 mm, the rate of change of temperature gradient on both sides of the scanning line decreases compared to that when  $\Delta X_{CL} = 0.7$  mm, and the symmetry of the temperature distribution increases. Figure 11b shows the influence of the relative distance  $\Delta X_{CY}$  between the laser spot center and the jet center on the temperature distribution perpendicular to the scanning direction at the crack front during the process of correcting the circular arc cutting path using low-temperature gas cooling when the laser scanning time is  $T = 3.2$  s. It can be observed that as  $\Delta X_{CY}$  increases, the temperature gradient on the inner side (center of the circle side) of the scanning line is significantly larger than that on the outer side (away from the center side of the circle), and when  $\Delta X_{CY} = 1$  mm, the position of the highest temperature deviates to the outside of the scanning line, causing a change in the direction of the temperature gradient on the outer side of the scanning line.

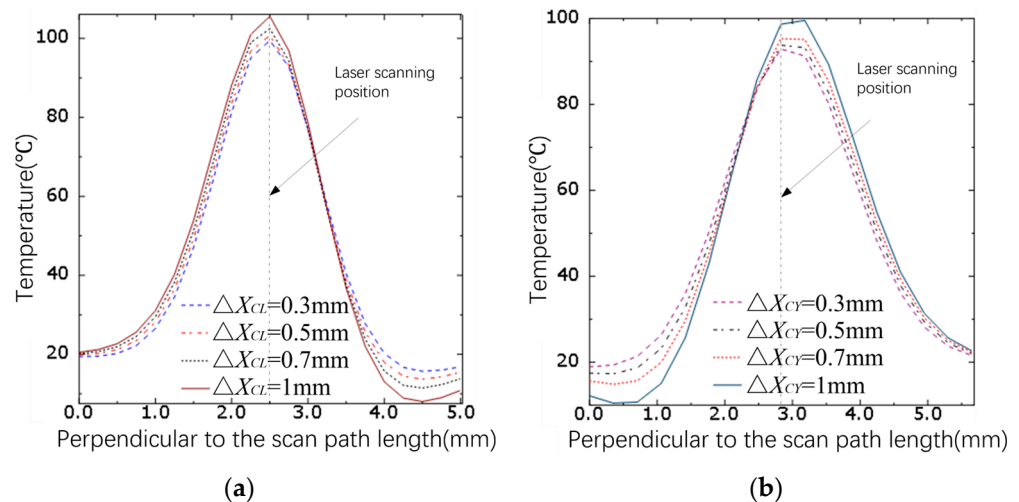


**Figure 11.** Temperature distribution graphs perpendicular to the scan path at the crack tip with the different transverse distance between the jet center and laser spot. (a) Asymmetric line; (b) circular arc curve.

The temperature field obtained from the low-temperature gas cooling trajectory correction technique described above is loaded into an extended finite element model to obtain the corresponding stress field distribution and crack propagation status. Figure 12 shows the stress field distribution of asymmetric cutting. Figure 13 shows the stress field distribu-

tion during crack propagation when the relative distance between the laser spot center and the jet center is  $\Delta X_{CL} = \Delta X_{CY} = 0.7$  mm. Compared with the stress field distribution before correction, low-temperature gas cooling increases the symmetry of the cutting process, and the compressive stress distribution on both sides of the crack is more symmetrical during the stable propagation stage.

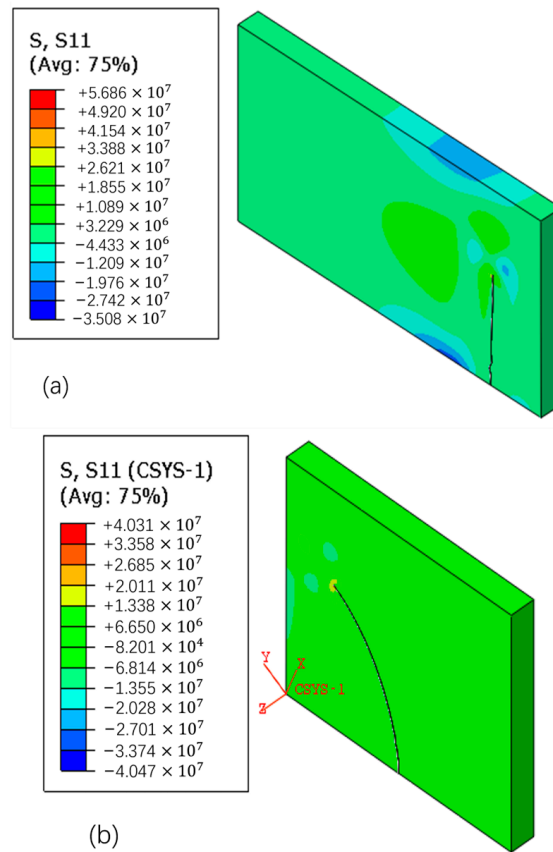


Figure 12. Stress field distributions of asymmetric cutting. (a) Asymmetric line; (b) circular arc curve.

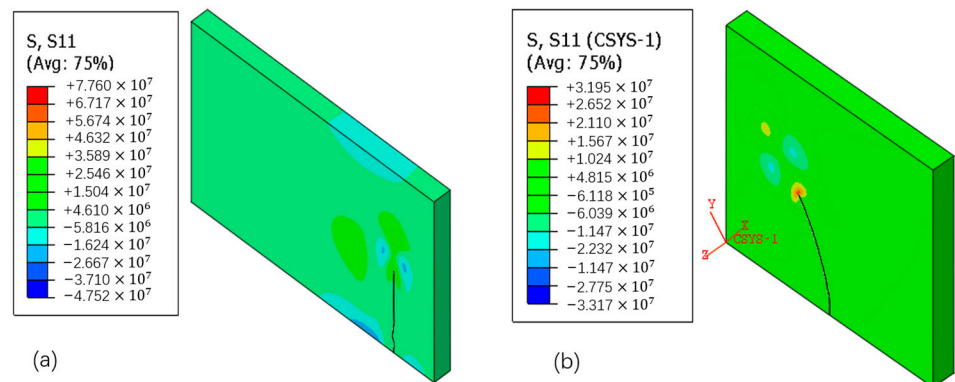
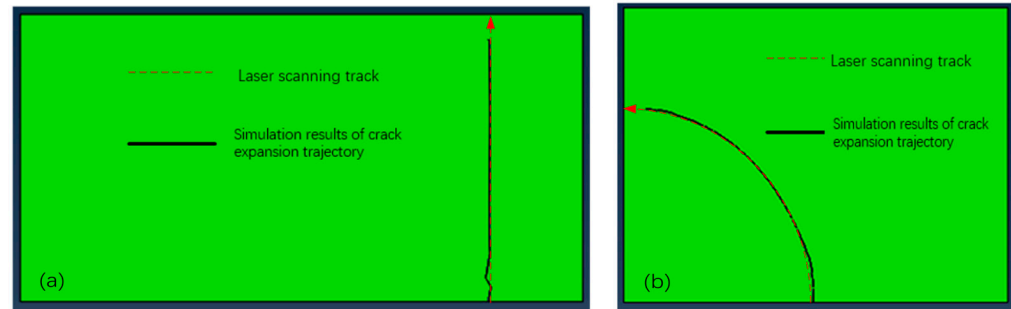


Figure 13. Stress field distributions of low-temperature gas cooled revising the trajectory deviation. (a) Asymmetric line; (b) circular arc curve.

Figure 14 shows the simulation results of the crack trajectory offset after low-temperature gas cooling trajectory correction. It can be seen that the crack propagation trajectory almost overlaps with the separated laser scanning trajectory, but in the initial stage of trajectory correction, the crack propagation is unstable due to the edge effect, and the crack trajectory shows some deviation. As the processing continues, low-temperature gas cooling can

effectively correct the trajectory deviation, and the overlap between the crack propagation trajectory in the stable stage and the laser scanning trajectory is higher.



**Figure 14.** Simulation result of low-temperature gas cooled revising the trajectory deviation. (a) Asymmetric line; (b) circular arc curve.

The stress distribution curve of the crack front perpendicular to the scanning direction during the correction of the asymmetric linear cutting trajectory by low-temperature gas cooling is shown in Figure 15. It can be seen that the compressive stress on the left side of the scan line is greater than that on the right side due to the edge effect at the beginning and end of processing, while the compressive stress on the right side is greater than that on the left side at the stabilization section, and the difference between the compressive stresses on both sides of the scan line is smaller, which is beneficial to the trajectory correction. During the whole processing stage, the position of the minimum value of transverse shear force is basically maintained on the laser scan line, but the direction of transverse shear force changes at the end stage, which is due to the introduction of low-temperature cold air, which makes the temperature gradient in the scanning direction larger and the distance of the crack front lagging behind the laser spot smaller, and the crack front is closer to the edge of the material at the end section, and the effect of the edge is greater, thus changing the direction of the transverse shear force. Combining the distribution characteristics of tensile stress and transverse shear force, it can be seen that low-temperature air cooling can effectively correct the crack trajectory of asymmetric linear cutting in the stable extension section, but still cannot eliminate the effect of the edge effect, and the crack extension in the first and last sections is not stable.

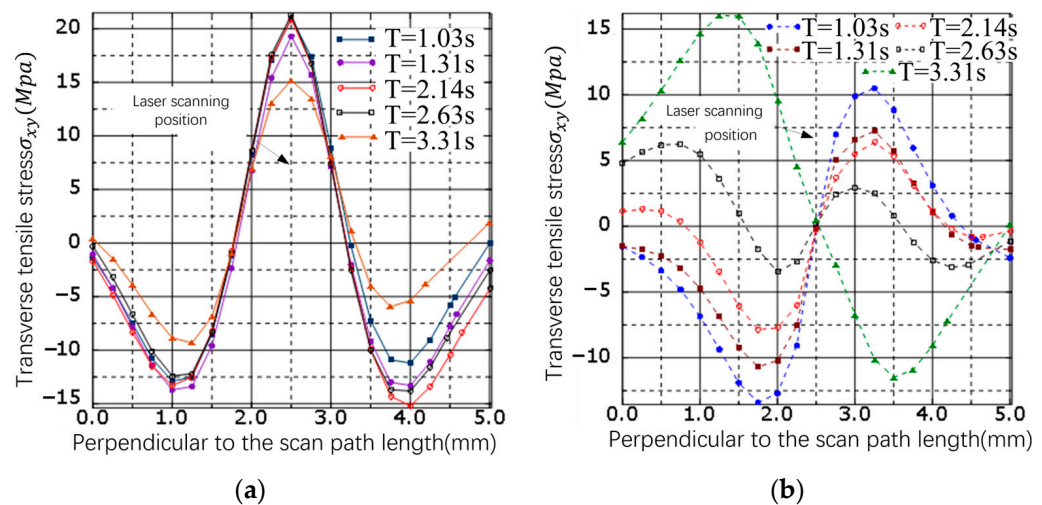


**Figure 15.** The stress distribution curve perpendicular to the scan path at the crack tip in low-temperature gas cooling revising the trajectory deviation for asymmetric linear cutting glass. (a) Tensile stress distribution curve. (b) Transverse shear stress distribution curve.

Figure 16 shows the stress distribution curve perpendicular to the scanning direction at the crack front during the process of correcting the circular arc cutting trajectory using low-temperature gas cooling. From the figure, it can be seen that in the initial stage, the compressive stress on the inner side of the laser scanning line is greater than that on the outer side of the arc, and the position of the minimum value of lateral shear force appears on the laser scanning line, which suppresses the unstable state of the crack in the initial stage to some extent. In the stable and final stages of trajectory correction, the compressive stress on both sides of the laser scanning line always shows that the inner side of the arc is smaller than the outer side, which is beneficial for trajectory correction. The position of the minimum value of lateral shear force appears on the separated laser scanning line in the stable stage and deviates from the laser scanning line position in the final stage.

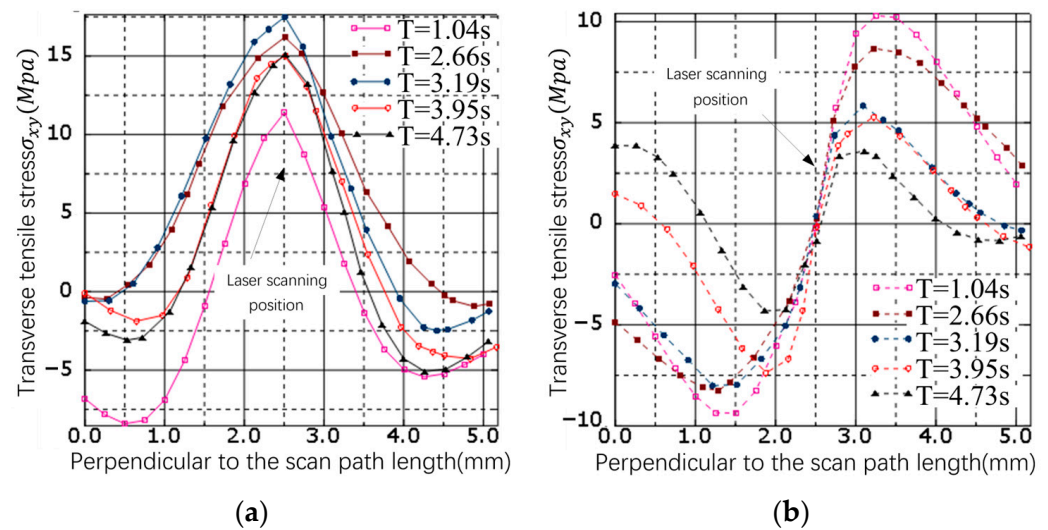
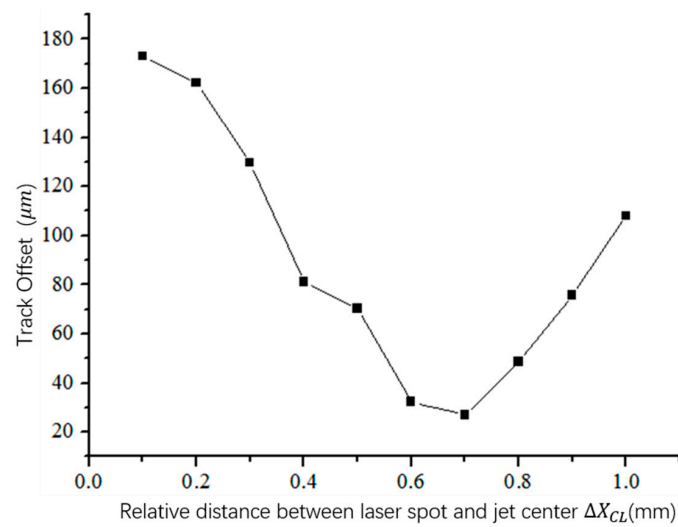


**Figure 16.** The stress distribution curve perpendicular to the scan path at the crack tip in low-temperature gas cooling revising the trajectory deviation for circular arc cutting glass. (a) Tensile stress distribution curve; (b) transverse shear stress distribution curve.

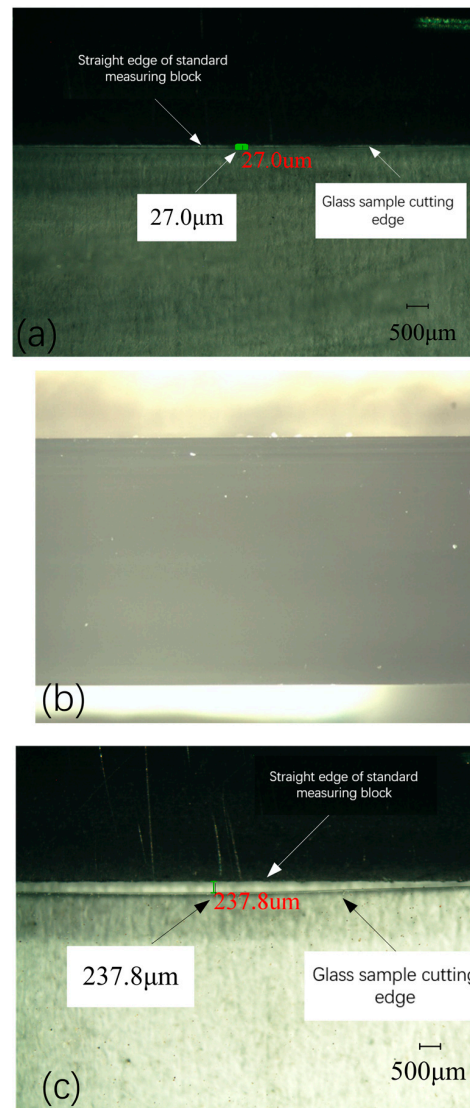
Based on the simulation results obtained, experimental research on trajectory correction using low-temperature gas cooling was conducted by changing the relative position relationship between the jet center and the laser spot center.

Figure 17 shows the correction effect of the deviation of the asymmetric straight cutting trajectory with respect to the relative distance  $\Delta X_{CL}$  is between the laser spot center and the jet center. It can be seen that the trajectory deviation decreases first and then increases with the increase of  $\Delta X_{CL}$ . Low-temperature gas cooling is applied to the right side of the scanning line, which increases the temperature gradient on the right side of the scanning line and promotes the position of the minimum value of lateral shear force to approach the scanning line. When  $\Delta X_{CL}$  is 0.7 mm, the temperature gradient on both sides of the scanning line is the largest, the temperature distribution is the most asymmetrical, and the trajectory deviation is the smallest, achieving the best trajectory correction. At the same time, when  $\Delta X_{CL}$  is 0.6 mm and 0.8 mm, the trajectory deviations are both below 50  $\mu\text{m}$ , which can effectively reduce the deviation of the cutting trajectory.

Figure 18 shows the best correction effect of the low-temperature gas cooling trajectory correction technology, with a minimum trajectory deviation of 27  $\mu\text{m}$  and high-quality separation surface. This is because the low-temperature gas cooling trajectory correction technology introduces a cooling mechanism based on the original separation laser, making the stress change during the crack propagation process smoother, resulting in a better-quality separation surface.



**Figure 17.** Deviations of separation path in low-temperature gas cooling revising the trajectory deviation for asymmetric linear cutting glass.



**Figure 18.** Best revised result in low-temperature gas-cooled revising technology. (a) Minimum trajectory deviation; (b) Cutting surface quality; (c) Asymmetric cutting.

Figure 19 shows the correction effect of the different relative distances of the laser optical axis and jet center  $\Delta X_{CY}$  on the cutting trajectory of the circular arc curve. It can be seen that the minimum trajectory offset after correction appears at  $\Delta X_{CY} = 0.7$  mm, when  $\Delta X_{CY} < 0.7$  mm, with the increase of  $\Delta X_{CY}$ , the inner temperature gradient of the scan line becomes larger and the outer temperature gradient becomes smaller, the asymmetry of temperature distribution increases and the trajectory offset decreases, but when  $\Delta X_{CY} > 0.7$  mm, with the further increase of  $\Delta X_{CY}$ , the outer temperature gradient of the scan line direction changes and the trajectory offset becomes larger.

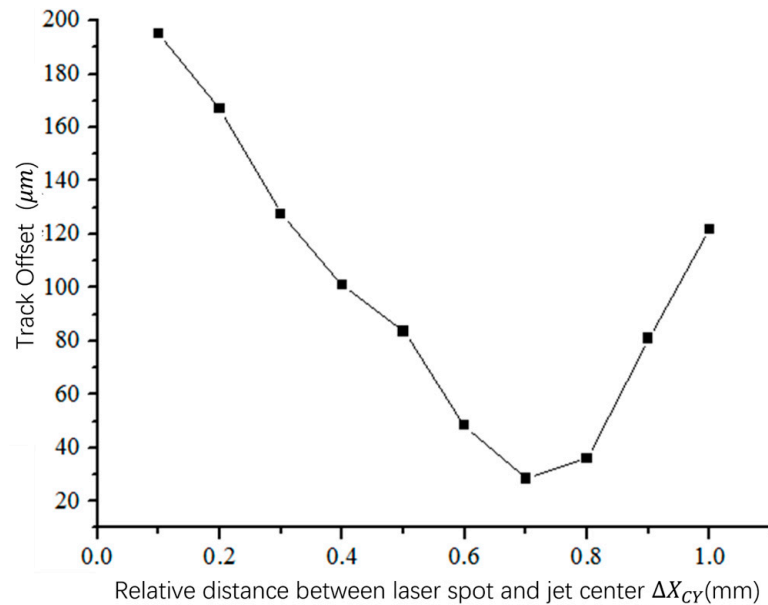


Figure 19. Deviations of separation path in low-temperature gas cooling revising the trajectory deviation for circular arc cutting glass.

Figure 20 shows the correction effect of the low-temperature gas cooling trajectory correction technology on a cutting arc with a radii of  $R = 5$  mm and  $R = 10$  mm. The trajectory deviation after correction for the  $R = 5$  mm arc radius is  $27.0 \mu\text{m}$ , and for the  $R = 10$  mm arc radius is  $28.5 \mu\text{m}$ , indicating a better correction effect for a smaller cutting arc radius. This is because the introduction of low-temperature gas increases the temperature gradient in the scanning direction, reducing the distance between the crack front and the laser spot. Without considering the influence of other correction effects, the smaller the distance between the crack and the laser, the closer the crack extension trajectory is to the laser scanning trajectory during the process of machining the circular arc curve, reducing the trajectory deviation compared to the asymmetric case (show in the Figure 21).

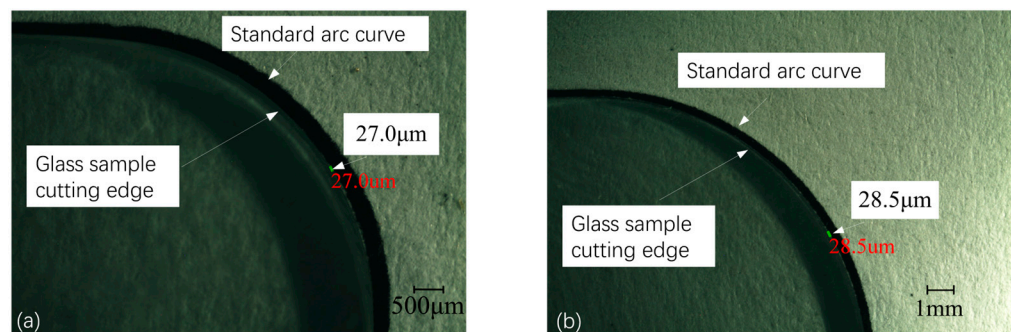
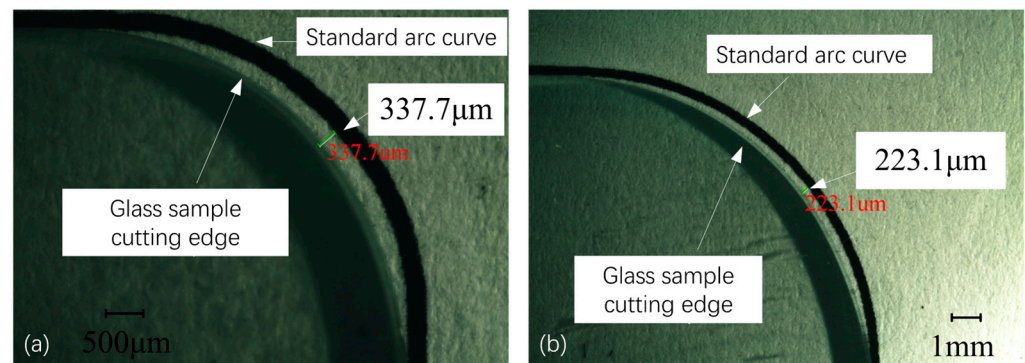


Figure 20. Best revised results with different cutting arc radius in low-temperature gas cooling revising the trajectory deviation technology. (a)  $R = 5$  mm; (b)  $R = 10$  mm.



**Figure 21.** Trajectory offsets for different arc radius cuts under asymmetry. (a)  $R = 5$  mm; (b)  $R = 10$  mm.

## 5. Conclusions

To conclude, the trajectory correction technique of cryogenic gas cooling is proposed for the trajectory shift problem that occurs in the stable extension stage in the asymmetric cutting commonly processed in laser-induced thermal crack propagation (LITP). Through a finite element simulation of the effect of cryogenic gas cooling on the temperature field distribution during the trajectory correction process, it is concluded that during the trajectory of asymmetric linear cutting, cryogenic gas cooling loaded on the side with less material in the stable expansion section can effectively correct the crack trajectory of asymmetric linear cutting, and the compressive stress on both sides of the laser scan line in circular arc cutting always shows that the inner side of the arc is smaller than the outer side of the arc, and cryogenic gas cooling. In the stable extension section, loading on the inner side of the arc can effectively correct the crack trajectory of asymmetric linear cutting. The test was carried out by the constructed low-temperature gas cooling system. The results show that in the trajectory correction technique for asymmetric linear cutting, cryogenic gas is injected on the side with less material in the scan line, while in the trajectory correction technique for circular arc curve cutting, cryogenic gas is injected on the inner side of the circular arc curve. The optimal relative distance between the center of its cooling gas and the center of the laser spot are both  $\Delta X_{CL} = \Delta X_{CL} = 0.7$  mm. For asymmetric linear cutting, the corrected minimum offset is  $27 \mu\text{m}$ , while for the circular arc curve cutting the smaller the radius is, the better the correction small effect is; at  $R = 5$  mm, the offset is  $27 \mu\text{m}$ . The analysis of experimental results and numerical simulation results shows that the low-temperature gas cooling correction trajectory offset technology can effectively revise the deviation of the separation path in asymmetry linear cutting glass with LITP.

The results of this paper have important implications for improving the application rate of LITP technology in practical glass processing. However, in order to expand the application of this technology, more work is needed to investigate closed shaped cutting with LITP.

**Author Contributions:** C.Z.: Conceptualization, writing—original draft preparation, funding acquisition. Z.Y.: methodology, software, investigation. X.Q.: Investigation, supervision. J.S.: Supervision, writing—review and editing, funding acquisition. Z.Z.: Data curation, funding acquisition. All authors have read and agreed to the published version of the manuscript.

**Funding:** This research was funded by the National Natural Science Foundation of China (Grant No. 62003216); the National Natural Science Foundation—Aerospace Joint Fund (Grant No. U2037205); the Natural Science Foundation of Guangdong Province (Grant No. 2022 A1515010600); the Guangdong Basic and Applied Basic Research Foundation (2020A1515111011); Shenzhen University stability support plan (Grant No. 20200814105908002, 20220809212220001); and the Shenzhen Top Talents Start-Up Fund (Grant No. 000711).

**Institutional Review Board Statement:** Not applicable.

**Informed Consent Statement:** Not applicable.

**Data Availability Statement:** Not applicable.

**Conflicts of Interest:** No conflicts of interest exist in this submitted manuscript, and the manuscript was approved by all authors for publication. I would like to declare on behalf of my co-authors that the work described was original research that has not been published previously, and not under consideration for publication elsewhere, in whole, or in part.

## References

1. Zheng, H.Y.; Lee, T. Studies of CO<sub>2</sub> laser peeling of glass substrates. *J. Micromech. Microeng.* **2005**, *15*, 2093. [[CrossRef](#)]
2. Solinov, E.F.; Solinov, V.F.; Buchanov, V.V.; Kustov, M.E.; Murav'ev, É.N. Application of laser technology for cutting glass articles. *Glass Ceram.* **2015**, *71*, 306–308. [[CrossRef](#)]
3. Kuo, Y.L.; Lin, J. Laser cleaving on glass sheets with multiple laser beams. *Opt. Lasers Eng.* **2008**, *46*, 388–395. [[CrossRef](#)]
4. Nisar, S.; Li, L.; Sheikh, M.A. Laser glass cutting techniques—A review. *J. Laser Appl.* **2013**, *25*, 042010. [[CrossRef](#)]
5. Zhimalov, A.B.; Solinov, V.F.; Kondratenko, V.S.; Kaplina, T.V. Laser cutting of float glass during production. *Glass Ceram.* **2006**, *63*, 319–321. [[CrossRef](#)]
6. Tsai, C.H.; Huang, B.W. Diamond scribing and laser breaking for LCD glass substrates. *J. Mater. Process. Technol.* **2008**, *198*, 350–358. [[CrossRef](#)]
7. Pan, C.T.; Hsieh, C.C.; Su, C.Y.; Liu, Z.S. Study of cutting quality for TFT-LCD glass substrate. *Int. J. Adv. Manuf. Technol.* **2008**, *39*, 1071–1079. [[CrossRef](#)]
8. Zhou, M.; Ngoi BK, A.; Yusoff, M.N.; Wang, X.J. Tool wear and surface finish in diamond cutting of optical glass. *J. Mater. Process. Technol.* **2006**, *174*, 29–33. [[CrossRef](#)]
9. Jia, X.; Li, K.; Li, Z.; Wang, C.; Chen, J.; Cui, S. Multi-scan picosecond laser welding of non-optical contact soda lime glass. *Opt. Laser Technol.* **2023**, *161*, 109164. [[CrossRef](#)]
10. Lai, S.; Ehrhardt, M.; Lorenz, P.; Zajadacz, J.; Han, B.; Lotnyk, A.; Zimmer, K. Ultrashort pulse laser-induced submicron bubbles generation due to the near-surface material modification of soda-lime glass. *Opt. Laser Technol.* **2022**, *146*, 107573. [[CrossRef](#)]
11. Mingareev, I.; Bautista, N.; Yadav, D.; Bhandari, A. Ultrafast laser deposition of powder materials on glass. *Opt. Laser Technol.* **2023**, *160*, 109078. [[CrossRef](#)]
12. Finucane, M.A.; Black, I. CO<sub>2</sub> laser cutting of stained glass. *Int. J. Adv. Manuf. Technol.* **1996**, *12*, 47–59. [[CrossRef](#)]
13. Liang, L.; He, L.; Jiang, Z.; Tan, H.; Jiang, C.; Li, X. Experimental study on the direct planar metallization on glass by the particle sputtering in laser-induced plasma-assisted ablation. *J. Manuf. Process.* **2022**, *75*, 573–583. [[CrossRef](#)]
14. Cai, Y.; Yang, L.; Zhang, H.; Wang, Y. Laser cutting silicon-glass double layer wafer with laser induced thermal-crack propagation. *Opt. Lasers Eng.* **2016**, *82*, 173–185. [[CrossRef](#)]
15. Lumley, R.M. Controlled separation of brittle materials using a laser. *Ceram. Bull.* **1969**, *48*, 850.
16. Zhao, C.; Zhang, H.; Wang, Y. Semiconductor laser asymmetry cutting glass with laser induced thermal-crack propagation. *Opt. Lasers Eng.* **2014**, *63*, 43–52. [[CrossRef](#)]
17. Zhao, C.; Cai, Y.; Ding, Y.; Yang, L.; Wang, Z.; Wang, Y. Investigation on the crack fracture mode and edge quality in laser dicing of glass-anisotropic silicon double-layer wafer. *J. Mater. Process. Technol.* **2020**, *275*, 116356. [[CrossRef](#)]
18. Kang, H.S.; Hong, S.K.; Oh, S.C.; Choi, J.-Y.; Song, M.-G. Cutting glass by laser. In Proceedings of the Second International Symposium on Laser Precision Microfabrication, Singapore, 16–18 May 2001; Volume 4426, pp. 367–370.
19. Nisar, S.; Sheikh, M.A.; Li, L.; Safdar, S. Effect of thermal stresses on chip-free diode laser cutting of glass. *Opt. Laser Technol.* **2009**, *41*, 318–327. [[CrossRef](#)]
20. Zhao, C.; Zhang, H.; Yang, L.; Wang, Y.; Ding, Y. Dual laser beam revising the separation path technology of laser induced thermal-crack propagation for asymmetric linear cutting glass. *Int. J. Mach. Tools Manuf.* **2016**, *106*, 43–55. [[CrossRef](#)]
21. Ogata, K.; Nagato, K.; Ito, Y.; Nakano, H.; Hamaguchi, T.; Saito, I.; Fujiwara, T.; Nagata, T.; Ito, Y.; Nakao, M. Real-time observation of crack propagation and stress analysis during laser cutting of glass. *J. Laser Appl.* **2019**, *31*, 042008. [[CrossRef](#)]
22. Yang, L.J.; Wang, Y.; Tian, Z.G.; Cai, N. YAG laser cutting soda-lime glass with controlled fracture and volumetric heat absorption. *Int. J. Mach. Tools Manuf.* **2010**, *50*, 849–859. [[CrossRef](#)]
23. Singh, D.; Premachandran, B.; Kohli, S. Experimental and numerical investigation of jet impingement cooling of a circular cylinder. *Int. J. Heat Mass Transf.* **2013**, *60*, 672–688. [[CrossRef](#)]
24. Nouri-Bidgoli, H.; Ashjaee, M.; Yousefi, T. Experimental and numerical investigations on slot air jet impingement cooling of a heated cylindrical concave surface. *Heat Mass Transf.* **2014**, *50*, 437–448. [[CrossRef](#)]
25. Jacob, A.; Leena, R.; Krishnakumar, T.S. Numerical and Experimental Investigations on Jet Impingement Cooling. *Int. J. Mech. Mechatron. Eng.* **2013**, *7*, 516–520.

**Disclaimer/Publisher's Note:** The statements, opinions and data contained in all publications are solely those of the individual author(s) and contributor(s) and not of MDPI and/or the editor(s). MDPI and/or the editor(s) disclaim responsibility for any injury to people or property resulting from any ideas, methods, instructions or products referred to in the content.